ACS OMEGA

Open Access

http://pubs.acs.org/journal/acsodf

Article

Optical Sensor Based on WS_2 Quantum Dots for Lamotrigine Determination

Lina Hristova, Rut Martínez-Moro, Esperanza Fernández-García, Luis Vázquez, Pedro Atienzar, María Dolores Petit-Domínguez, Elena Casero, Carmen Quintana, and María del Pozo*

Cite This: *ACS Omega* 2025, 10, 17257−17268

Read Online

ACCESS | Metrics & More | Article Recommendations | Supporting Information

ABSTRACT: In this work, we obtained WS_2 quantum dots by both liquid exfoliation and hydrothermal synthesis following a top-down and a bottom-up approach, respectively. The resulting nanomaterials were spectroscopically characterized by UV−vis absorption and fluorescence techniques. Atomic force microscopy measurements were performed for the morphological characterization. We have studied the interaction between the as-synthesized WS_2 quantum dots with the antiepileptic drug lamotrigine, a noncolored analyte. This interaction produces a quenching of the native fluorescence of the nanomaterials, which depends linearly on the lamotrigine concentration. Moreover, the Stern−Volmer constants were calculated and the inhibition mechanism of the interaction was also investigated. Next, the WS_2 quantum dots were immobilized on quartz supports for the development of an optical sensor for lamotrigine determination. The sensor shows a linear response with the analyte concentration in the 35.4−250 μM range, with a limit of detection of 10.6 μM. The sensor was applied to the determination of lamotrigine in a synthetic serum sample, obtaining a recovery of 94%. Moreover, for a rapid and visual detection of lamotrigine, we have tested the suitability of using paper as a support for immobilizing WS_2 quantum dots.

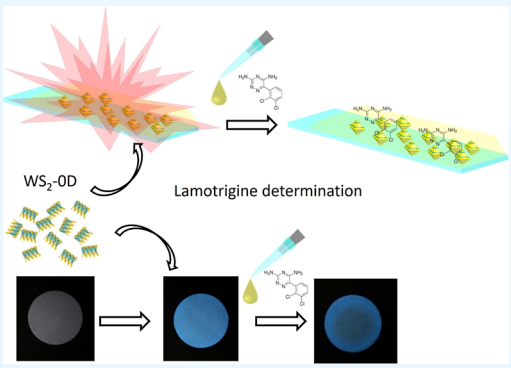

INTRODUCTION

The excellent results obtained from the employment of graphene in applications related to energy generation and storage, catalysis or chemical sensors have prompted the search for other low-dimensional materials.[1,2] Among them, transition metal dichalcogenides (TMDs) have garnered significant interest due to their unique properties and applications.[3] These materials exhibit a sandwich-like MX_2 structure, where M corresponds to a transition metal and X represents an element from the chalcogen group, typically a sulfur atom. A TMD sheet is formed by a layer of transition metal atoms bonded to two layers of chalcogen through covalent bonds. The different sheets interact with each other through weak van der Waals interactions, forming the 3D structure. These weak forces allow the 3D TMD to be easily exfoliated in 2D sheets by different methods.[4−6] By reducing the size of these sheets below 10 nm, zero-dimensional TMDs (quantum dots, QDs), can be obtained.[7] These 0D materials possess a higher surface-to-volume ratio and a higher number of active sites than sheets, which make them suitable for sensor development, catalysis processes, and bioimaging.[8,9] One of the most interesting properties of QDs is their photoluminescence, which contrasts with those of the bulk material and sheets. This is due to their quantum confinement and edge effects, which cause TMDs to exhibit a modulable bandgap depending on their size. The bandgap changes from direct, in the bulk material, to indirect as the dimension is reduced.[10,11]

The methods employed for the synthesis of TMDs QDs can be divided into two groups: top-down and bottom-up approaches.[7,12] Within the top-down methods, liquid exfoliation and ion-intercalation-assisted exfoliation stand out. The latter involves lengthy processes that require a purification step. In addition, the dots obtained by this method may have their semiconducting properties diminished due to the intercalation of Li or K ions.[12] Then, the method most employed to obtain the QDs is the exfoliation of the corresponding bulk material in suitable solvents, such as *N*-methyl-pyrrolidone (NMP) or dimethylformamide (DMF),[13] followed by a thermal treatment. This method is cost-effective, versatile, simple, and scalable.

On the other hand, bottom-up methods for the synthesis of TMD dots, especially WS_2, are less common.[12,14] Among others, chemical vapor deposition and hydrothermal reactions from precursors have been described. The latter is receiving

Received: October 17, 2024
Revised: February 10, 2025
Accepted: March 20, 2025
Published: April 25, 2025

more attention because it offers significant advantages, particularly in terms of environmental economics. Additionally, it is simple and allows control over the size of the dots depending on the reaction conditions.[8,14,15] However, it is worth noting that many hydrothermal synthesis methods yield polydisperse nanomaterials,[8,12,14] and impurities in the form of carbon dots may be formed due to the use of organic molecules as precursors.[16] This is reflected in the dependence of the maximum emission wavelength of the TMD QDs on the excitation wavelength.

The characteristic photoluminescence of these materials has driven the development of optical analytical methodologies that exploit fluorescence inhibition that occurs when the nanomaterial interacts with a given analyte. These methods offer numerous advantages such as excellent sensitivity, selectivity, simplicity, and quickness.[17] Among the TMDs family, molybdenum disulfide and tungsten disulfide are particularly noteworthy for this kind of applications. Numerous studies have focused on the fluorescence inhibition of MoS_2 QDs when interacting with analytes such as the food dye allura red,[18] methotrexate,[19] nitrobenzene,[20] or fluorine ions.[21] Similarly, methods using WS_2 QDs have also been developed. In these works, different synthesis strategies have been employed. For instance, most examples used WS_2 QDs synthesized via the hydrothermal method, which were applied for the determination of trypsin and dithiothreitol,[22] dopamine,[23] hydrogen peroxide,[24] nitrofurazone,[25] and ofloxacin and ciprofloxacin.[26] Furthermore, Azizi et al. have reported the fluorometric and smartphone-based colorimetric sensor for cyanide detection employing WS_2 QDs and silver nanoparticles.[27] Additionally, WS_2 QDs synthesized using a top-down strategy in DMF have been employed for nonenzymatic electrochemiluminescence-based detection organophosphorus pesticides[28] and in combination with fluorescein for the analysis of cefixime residues in milk.[29]

Although most fluorescence methods based on the use of TMD QDs are designed for analysis in solution, an interesting alternative is their incorporation into a solid support. Paper-based analytical devices have demonstrated significant potential for sensor development due to their convenience, low cost, and portability. Since paper is a disposable material, this technology offers several advantages, including rapid diagnostic, scalability, biocompatibility, ease of use, and functionalization.[30] In these designs, the inhibition of the signal due to the interaction with the analyte is observed under irradiation with a hand-held UV light lamp. Additionally, the ability to use a smartphone or digital camera for analyte detection makes a paper-based sensor simple, environmentally friendly, portable, and cost-effective.[31] It has been shown that paper-based devices allow on-site analyte evaluation with fast response time, high sensitivity, and good specificity.[32,33]

However, this approach is still in its early stages, all of the optical sensors being proposed based on the use of MoS_2. These sensors are applied to the determination of analytes such as trinitrotoluene (TNT),[33] Hg^{2+} ions,[34] and the fungicide fluazinam.[35] In addition to conducting studies in solution, these works have shown the possibility of incorporating MoS_2 QDs onto paper or quartz supports, showing responses to different analyte concentrations.[34,36] This opens the door to the development of simple sensors for "in situ" analysis.

Epilepsy is a chronic neurological disorder caused by the abnormal firing of brain neurons. It leads to transient brain dysfunction, significantly impacting the health and psychosocial well-being of patients.[37] One of the antiepileptic drugs used for the treatment of seizures is lamotrigine, which is used to prevent or reduce the severity of epileptic attacks in children, the elderly, and pregnant women.[38] The recommended serum concentration of lamotrigine is between 1 and 4 μg/mL.[39] However, the blood levels of lamotrigine can be affected by various factors such as age, renal, and hepatic function, genetic background, and drug interactions.[38] Since maintaining a constant concentration of the drug in the patient's blood is crucial to optimizing their treatment and avoiding toxic effects, therapeutic drug monitoring is extremely important. Therefore, it is necessary to develop sensitive, rapid, and accurate analytical methods to determine lamotrigine levels in the blood.

Most of the analytical methods found in the literature for lamotrigine determination are based on high-performance liquid chromatography coupled with mass spectrometry or UV−vis detectors.[37−41] An alternative to the expensive and laborious chromatography-based methods is the use of optical sensors based on fluorescence, as they are simple and cost-effective and provide high sensitivity. Concerning lamotrigine determination by electrochemical techniques, a few examples can be found in the literature.[42,43] Since lamotrigine is a nonfluorescent compound, various strategies for fluorescence detection have been developed. For instance, El-Enany et al. developed a spectrofluorimetric method based on the derivatization of the drug with the fluorophore *o*-phthalaldehyde.[44] Most of the methodologies developed to date are based on the intensity inhibition of a nanomaterial or polymer as fluorescent probes, with several examples available in the literature. For instance, Song et al. synthesized a fluorescent terbium-based coordination polymer that interacts with lamotrigine, enabling its detection.[45] Additionally, various metal−organic framework nanostructures, including those based on lanthanide[46] or terbium,[47] have been reported for lamotrigine determination. Related with quantum dots-based nanomaterials, N-doped graphene carbon nanodots[48] or gold quantum dots and silver nanoparticles[49] have also been proposed for this purpose. It is also important to note that in these works, the lamotrigine determination was conducted in solution conditions. Therefore, the development of an optical sensor on a solid support that allows rapid lamotrigine detection should garner great interest. In this work, we present for the first time the employment of WS_2 QDs for lamotrigine determination. Moreover, based on our recent experience in immobilizing MoS_2 on quartz employing a polymeric membrane,[36] we propose applying this strategy to develop an optical sensor for lamotrigine determination based on its interaction with WS_2 QDs.

EXPERIMENTAL SECTION

Reagents and Materials. Tungsten disulfide 90 nm (99%), sodium tungstate dihydrate ($Na_2WO_4{\cdot}2H_2O$), L-cysteine, polyvinyl chloride (PVC), tributyl phosphate (TBP), dimethyl sulfoxide (DMSO), synthetic human serum, and lamotrigine were purchased from Sigma-Aldrich (USA). NMP, tetrahydrofuran (THF), sulfuric acid, and sodium hydroxide were supplied from Scharlau Chemie (Spain).

Quartz planar plates were obtained from Vidrasa S.A. and cut into small pieces of 37 × 41 mm. Circular qualitative filter papers Whatman grade 1 of 2.5 cm diameter supplied by GCE

https://doi.org/10.1021/acsomega.4c09476
ACS Omega 2025, 10, 17257−17268

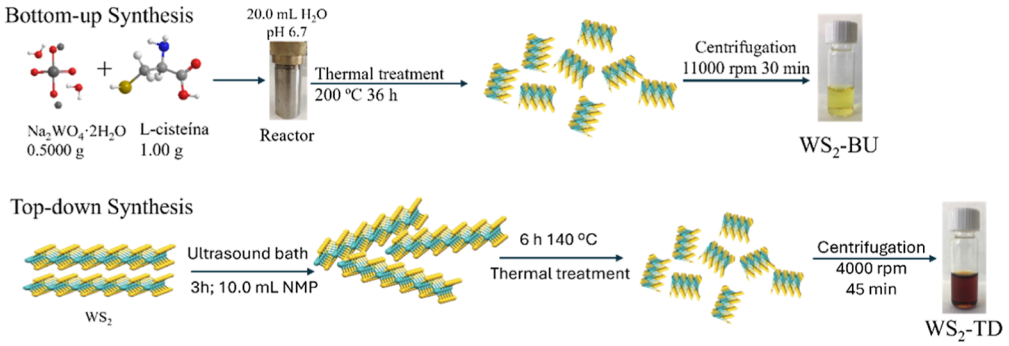

Figure 1. Schematic representation of bottom-up and top-down synthesis approaches.

Healthcare (UK) were employed for the development of paper sensors.

Instrumental Techniques. Fluorescence measurements were carried out with a Hitachi F-7000 spectrofluorometer equipped with a solid sample holder. Absorbance measurements were performed with a Shimadzu UV-1800 spectrophotometer. For the nanomaterials preparation, a Transonic 570/H (Elma) ultrasonic bath, a Rotofix 32 A (Hettich) centrifuge, and an oven (Nabertherm Inérica, S.L.) were employed. For the signal transduction with the paper-based sensor, a lamp of 365 nm (Darkbeam) was employed. The AFM measurements were carried out with a Nanoscope III (Veeco) system operating in the dynamic mode and using silicon cantilevers (Bruker) with a nominal radius of 8 nm and force constant close to 40 N/m. Lifetime measurements were recorded in an Edinburgh Instruments FLS1100 spectrofluorometer, which was coupled to a cooled photomultiplier (PMT-980).

Procedures. *WS_2 QDs Synthesis: Top-Down and Bottom-Up Approaches.* The synthesis of WS_2 QDs was carried out by two different methods as it is shown in Figure 1, top-down and bottom-up, based on literature with slight modifications.[8,50] For the top-down approach, 100 mg of commercial WS_2 was added to a flask containing 10.0 mL of NMP and subjected to exfoliation in an ultrasound bath for 3 h. After that, the suspension was heated under stirring at 140 °C in a silicon bath for 6 h and left to rest for 14 h. Next, the dots were separated in the supernatant by centrifugation at 4000 rpm for 45 min. The WS_2 QDs, named WS_2-TD, were stored under 4 °C until their use.

For the bottom-up synthesis, 0.5000 g of $Na_2WO_4{\cdot}2H_2O$ and 1.000 g of L-cysteine were dissolved in 10.0 mL of water and stirred for 30 min. Then, the pH was set at 6.65 with HCl 0.1 M and diluted to 20.0 mL in water. The mixture was transferred to a reactor and heated in an oven at 200 °C for 36 h. After centrifugation at 11,000 rpm for 30 min, the supernatant was separated and stored at 4 °C until its use. Hereafter, these WS_2-QDs are denoted as WS_2-BU.

AFM Measurements. To be able to image isolated structures, thus avoiding the formation of clusters, a drop of a diluted preparation of QDs (1:1000 in water) was deposited on top of a freshly cleaved mica surface. Thanks to the mica hydrophilicity, the drop was spread onto it, which also prevented the formation of QDs agglomerates. Once the drop was dried, the AFM measurements were taken at different locations. Due to tip convolution effects, the measured lateral size of the dots is not reliable since it is enlarged by the tip geometry. In contrast, the measured dot height is a meaningful datum because it is not affected by these effects. The QDs height distribution was obtained using the Gwyddion free-software.[51]

Spectroscopic Measurements. The spectroscopic measurements were carried out with an adequate dilution of the QDs in water. The absorbance measurements were recorded at between 200 and 800 nm. The fluorescence measurements were carried out under the optimal conditions for each nanomaterial. The excitation wavelengths were 270 and 310 nm for WS_2-TD and WS_2-BU, respectively.

The lifetime measurements were performed at room temperature utilizing a 294.8 nm excitation wavelength provided by a picosecond (ps) laser diode. The lifetimes (τ) were calculated from the best fitting of the signal to a single-exponential decay [$I(t) = I(0)\exp(-t/\tau)$].

The quantum yield was calculated employing quinine as the standard (Φ tabulated $\lambda_{exc275nm} = 0.577$) and according to the equation below

$$\phi_x = \phi_s \frac{A_s}{A_x} \cdot \frac{F_x}{F_s} \cdot \left(\frac{n_x}{n_s}\right)^2$$

Φ = fluorescence quantum yield, A = absorbance at λ_{exc}, F = emission curve area, n = solvent refraction index. Subscripts s and x correspond to the standard and the analyte, respectively.

Quartz-Based Fluorescence Sensor. The quartz plates were cleaned before modification as in a previous work.[52] Briefly described, the plates were rinsed with THF followed by 0.18 M H_2SO_4 solution and NaOH 1% (w/w) solution. Finally, the plates were rinsed with distilled water and dried at 40 °C.

For the incorporation of the QDs on the quartz surface, an optically transparent PVC-based membrane was prepared as follows: 35.00 mg of PVC was diluted in 790 μL of THF. Afterward, 100 μL of WS_2-BU and 110 μL of TBP as plasticizer were added to the mixture. The quartz modification was carried out by spin coating 75 μL of the mixture at 800 rpm for 1 min. The membranes were dried at 50 °C. In addition, membranes including 100 μL of THF instead of the nanomaterial were developed (membranes without WS_2-QDs denoted as blank membrane).

The lamotrigine determination was performed by adding 20 μL of the analyte solution to the sensor surface and drying it at 50 °C before the fluorescence measurement.

Paper-Based Fluorescence Sensor. Circular pieces of Whatman paper were submerged in the WS_2-BU suspension (diluted 1:10 in water) for 10 min. After drying at 30 °C in the oven, 25 μL of lamotrigine was added onto the center of the paper. Analytical detection was carried out by recording a picture under an excitation lamp of 365 nm.

https://doi.org/10.1021/acsomega.4c09476
ACS Omega 2025, 10, 17257−17268

RESULTS AND DISCUSSION

Nanomaterials Synthesis and Spectroscopic Characterization. The synthesis of WS_2 QDs was carried out by two different approaches top-down (WS_2-TD) and bottom-up (WS_2-BU) to evaluate if they present differences in their luminescence properties and, therefore, in their response toward lamotrigine. As described in the Experimental Section, the top-down approach was carried out from the bulk nanomaterial through the solvent exfoliation assisted by ultrasound and a subsequent temperature treatment. Meanwhile, the bottom-up synthesis was carried out in a hydrothermal synthesis reactor from a tungsten salt. The spectroscopic characterization of both nanomaterials was performed by UV−vis absorbance and fluorescence measurements, and the results are depicted in Figure 2.

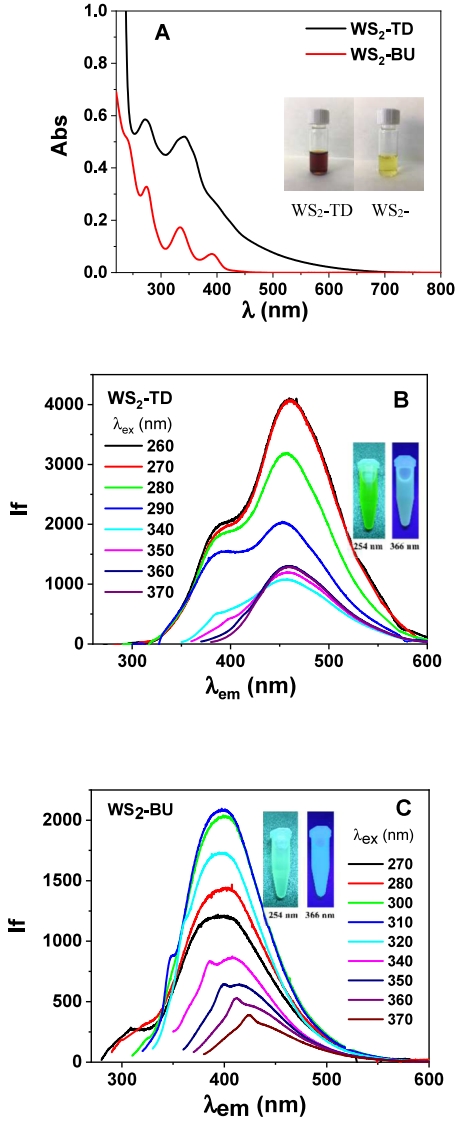

Figure 2. Spectroscopic characterization of the as-synthesized QDs. (A) UV−vis absorbance spectra of WS_2-TD and WS_2-BU at a dilution of 1:100 and 1:1500, respectively. The inset picture shows the as-synthesized WS_2-TD (left) and WS_2-BU (right). (B) Fluorescence spectra as a function of excitation wavelength of WS_2-TU at 1:100 dilution. (C) Fluorescence spectra as a function of excitation wavelength of WS_2-BU at 1:1500 dilution.

Figure 2A shows the absorbance spectra obtained for both nanomaterials. WS_2-TDs show two absorption bands centered at 270 and 340 nm, characteristic of the dots obtained by the top-down approach.[50] The same absorption bands are registered for WS_2-BU together with two additional bands around 240 and 400 nm which, according to the literature, is typical of QDs synthesized by bottom-up approaches.[8] The band obtained at 240 nm has been attributed to superficial defects and to the presence of functional groups such as $-NH_2$, $-SO_4^{2-}$, and $-OH^-$, among others. The presence of absorption bands at wavelengths below 400 nm and the absence of bands between 400 and 680 nm let us conclude that only dots but not WS_2 sheets were obtained.

As stated in the introduction section, one of the most interesting properties of QDs is their fluorescence emission. Figure 2B and C shows the fluorescence spectra at different excitation wavelengths for WS_2-TD and WS_2-BU QDs, respectively. As can be seen, irrespective of the synthesis approach, both nanomaterials present an emission fluorescence band, confirming the formation of WS_2 QDs.

In the case of WS_2-TD, this emission band is centered at 460 nm and exhibits the highest intensity when the excitation wavelength is 260−270 nm (see Figures 2B and S1A). The wavelength of the emission maximum does not change when different excitation wavelengths are applied, which indicates that the obtained dots present a homogeneous size.[53,54] In the case of WS_2-BU, the emission maximum is centered at 400 nm when the excitation wavelength is 310 nm (see Figures 2C and S1B). However, in this case, the λ emission maximum increases with the excitation wavelength. This bathochromic effect is in agreement with the results reported in the literature and it could be attributed to different sizes of WS_2-BU and to the presence of carbon dots coming from the precursors employed in the hydrothermal process.[53,54]

Additionally, the quantum yield of the synthesized materials was calculated using quinine sulfate as reference. The results obtained were 2.2% and 8.3% for WS_2-TD and WS_2-BU, respectively. Similar or even lower values have been reported for WS_2 dots in the literature.[12,24,29] Moreover, the lifetimes of WS_2-TD and WS_2-BU were also calculated, obtaining values of 2.24 and 5.97 ns, respectively. This small difference can be attributed to the size of the QDs or the presence of external defects. The obtained results are consistent with those reported in the literature.[22,24,25]

The spectroscopic characterization shows that both syntheses produce WS_2-QDs with differences in the excitation and emission wavelength. This characteristic difference makes each nanomaterial appropriate for interaction with specific analytes, allowing their determination.

Morphological Characterization by AFM. Figure 3A shows the AFM data obtained on the WS_2-TD. Some of the sample spots analyzed showed a large number of QDs. This allows to obtain a high number of features analyzed in the QDs height distribution shown in Figure 3B. We have fitted the data with the lognormal distribution, which has been reported to be followed by both nanoparticles[55] and QDs[56] size distributions. In this case, the fitting with lognormal is good around the peak. However, the data depart from the lognormal distribution for QD heights in the 0.5−1 nm range since they are larger than the fitted values. The average height is close to 0.4 nm. It should be noted that the continuous background layer of the image in Figure 3A shows a certain roughness that should come from the drop deposit since it should be noted that the

https://doi.org/10.1021/acsomega.4c09476
ACS Omega 2025, 10, 17257−17268

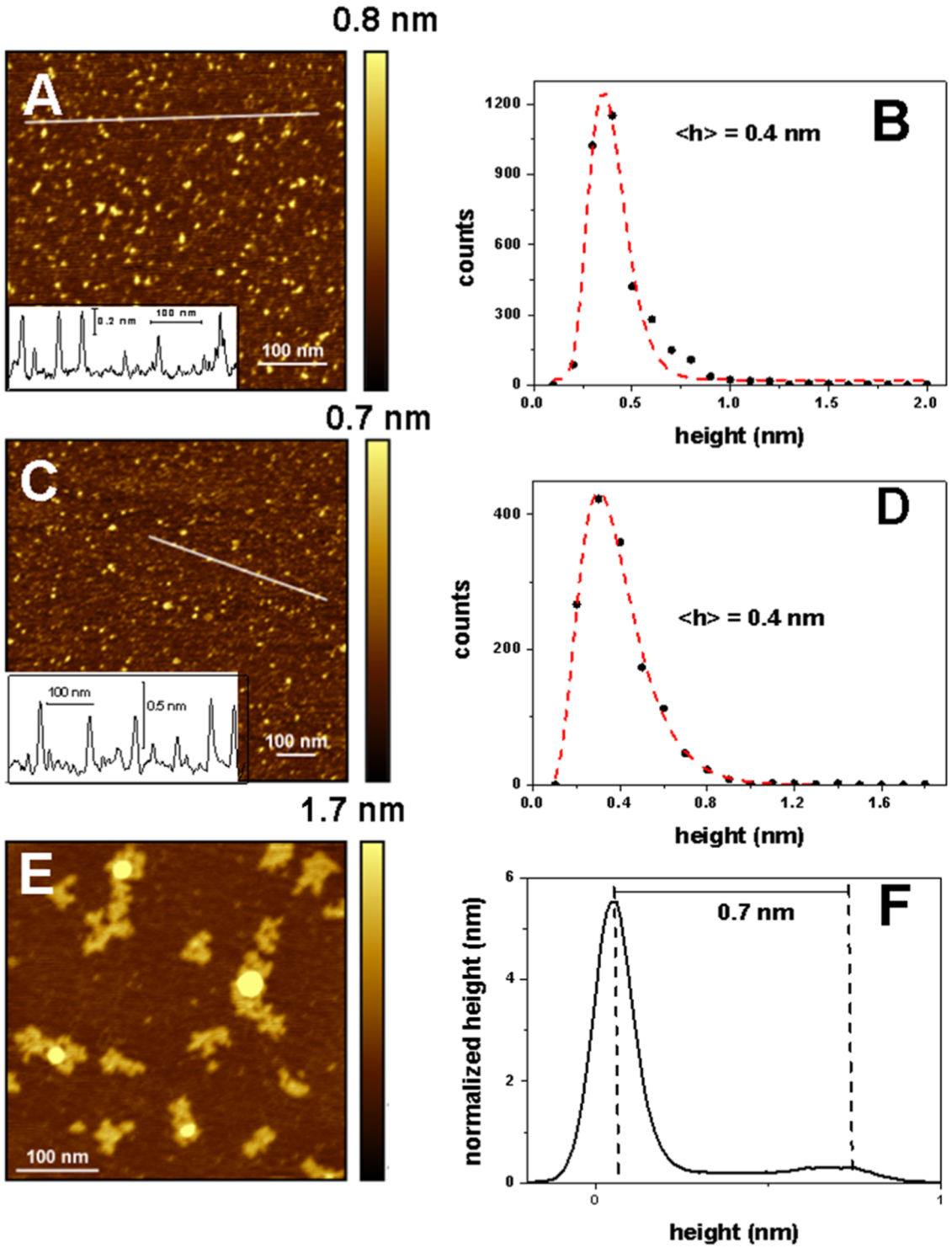

Figure 3. (A) AFM image of the WS_2-TD deposited on mica. The inset shows the surface profile along the line depicted in (A). (B) QDs height distribution obtained after analyzing several images. The dashed line is the best lognormal fit of the experimental data. (C) AFM image of a WS_2-BU deposited on mica. Inset: surface profile along the line depicted in (C). (D) QDs height distribution obtained after analyzing several AFM images. The dashed line is the best lognormal fit of the experimental data. (E) AFM image obtained on a zone where the WS_2-BU form small clusters. (F) Height distribution of (E).

bare mica surface is atomically flat (not shown). This is better appreciated in the surface profile shown in the inset. As explained above, this fact led to the employing of the threshold method to select the QDs and further analyze their height. This method likely underestimates the QDs heights. Furthermore, measurements (Figure S2) taken on regions where the background layer did cover partially the mica surface allowed us to estimate its thickness in the 1.5−2 nm range. Thus, from these facts (i.e., layer thickness and roughness), it can be stated that AFM underestimates the QDs height values.

Figure 3C shows a typical image obtained on the WS_2-BU sample. The bright spots correspond to WS_2 QDs. Between

https://doi.org/10.1021/acsomega.4c09476
ACS Omega 2025, 10, 17257−17268

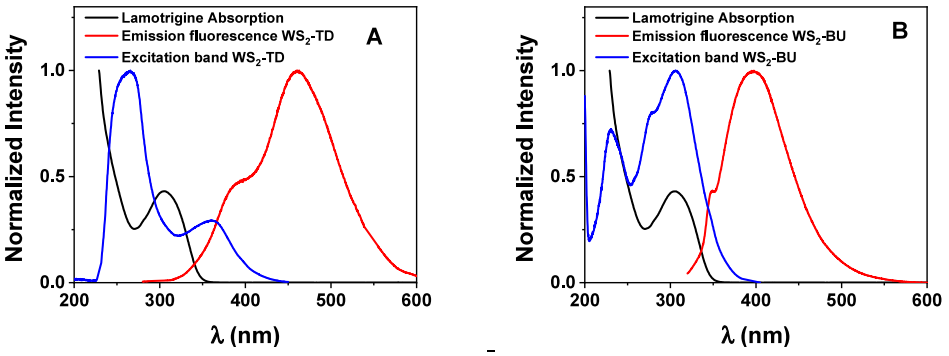

Figure 4. Absorption spectrum of lamotrigine and the excitation and emission spectrum of (A) WS_2-TD and (B) WS_2-BU.

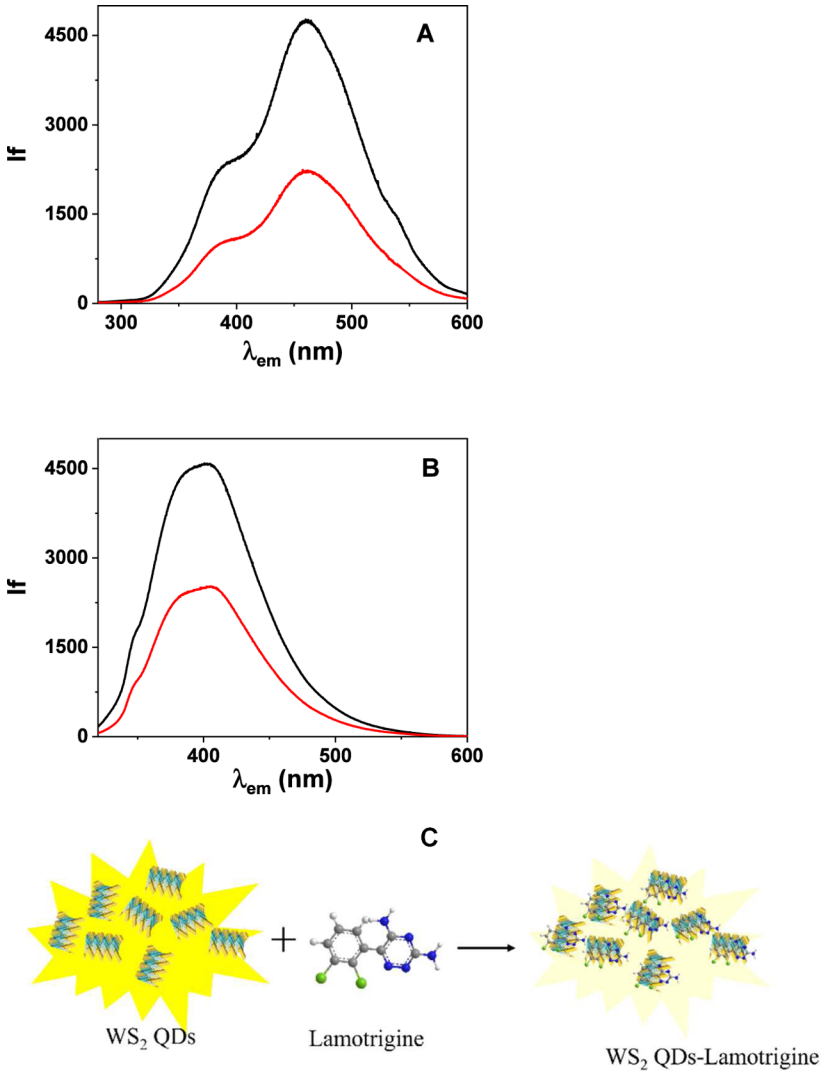

Figure 5. Fluorescence response of (A) WS_2-TD (λ_{ex} = 270 nm) and (B) WS_2-BU (λ_{ex} = 310 nm) in the absence (black spectra) and in the presence of 50 μM of lamotrigine (red spectra). (C) Schematic representation of the inhibition interaction process.

them, in the background, a certain corrugation is again observed. The height fluctuations found in this background are about 0.3−0.4 nm (see inset of Figure 3C). This fact implies that the QDs height values plotted in Figure 3D could be 0.3−0.4 nm higher. In this figure, it is shown that the QDs height distribution follows quite well a lognormal distribution. Note the large number of QDs that were analyzed. The average height value is close to 0.4 nm, which, taking into account the background roughness, could increase up to close to 0.8 nm.

Figure 3E shows the morphologies in other locations of the sample. Here, despite the diluted preparation, the QDs have aggregated in clusters. In this case, the surface is quite flat, without any substantial roughness. Inside the aggregates, the individual QDs can be distinguished. As the clusters have a quite homogeneous height and certain lateral extension, the

https://doi.org/10.1021/acsomega.4c09476
ACS Omega 2025, 10, 17257−17268

height distribution of the image (Figure 3F) shows two peaks. The higher one corresponds to the background, whereas the wider and lower one corresponds to the cluster structures. The distance between them indicates the average cluster height, which is close to 0.7 nm. This figure correlates well with that obtained from Figure 3D, once the correction due to the background roughness has been applied. Also note that in Figure 3E there are also three larger and higher (i.e., brighter) structures due to large QDs agglomerations with heights in the 3−4 nm range.

Finally, it is worth noting that whereas the WS_2-BU QDs size distribution does follow quite well a lognormal distribution, this is not the case for the WS_2-TD one, since the measured data for QDs sizes above the peak are larger than those fitted with the lognormal function. This difference in size distribution could be linked to their different optical behavior.

WS_2 QDs Interaction with Lamotrigine. As it was explained in the introduction section, we have selected lamotrigine, an antiepileptic drug, to demonstrate the applicability of WS_2-TD and WS_2-BU toward the determination of nonluminescence compounds. To evaluate whether the interaction between the nanomaterial and the selected analyte would be possible, we show in Figure 4A and B the lamotrigine absorption band together with the excitation and emission spectra of WS_2-TD and WS_2-BU, respectively. It should be noted that lamotrigine does not emit fluorescence when it is excited at its absorption wavelength or at the excitation wavelength employed with the WS_2-QDs nanomaterials (data not shown).

As can be observed, lamotrigine presents an absorption band with a maximum at 305 nm (black spectra) that slightly overlaps with the emission spectra (red spectra) of both nanomaterials. Moreover, the lamotrigine absorption band overlaps with the excitation band of both nanomaterials, being greater the overlapping between lamotrigine and WS_2-BU. The overlapping of the lamotrigine absorption spectrum with the spectra of WS_2-QDs allows us to expect the interaction between the lamotrigine and WS_2-QDs, leading to their fluorescence inhibition by an inner filter mechanism. To assess their interaction, fluorescence spectra of WS_2-QDs in the absence and presence of lamotrigine were recorded. Before carrying out these experiments, the nanomaterial dilution was adapted to get the same initial fluorescence intensity, obtaining 1:100 and 1:600 for WS_2-TD and WS_2-BU, respectively. Figure 5A and B shows the fluorescence spectra of each WS_2-QDs obtained in the absence and in the presence of 50 μM of lamotrigine. The fluorescence emission of both WS_2-TD and WS_2-BU is greatly quenched by the analyte, which confirms the interaction of both WS_2-QDs with lamotrigine.

In order to evaluate the degree of interaction between each nanomaterial and the lamotrigine as a quencher, the Stern−Volmer constant (K_{SV}) was determined for both WS_2-TD-lamotrigine and WS_2-BU-lamotrigine pairs. For this, we employed the Stern−Volmer equation ($I_{f0}/I_f = 1 + K_{SV}$ [lamotrigine]), where I_{f0} and I_f correspond to the emission intensity of WS_2-QDs in the absence and presence of the analyte, respectively. From the slope of the corresponding plot of I_{f0}/I_f against lamotrigine concentration, the K_{SV} value is obtained. The higher the K_{SV} value, the stronger the interaction. From the results shown in Figure S3, K_{SV} values of 20,431 and 17,556 M^{-1} were obtained for WS_2-TD-lamotrigine and WS_2-BU-lamotrigine, respectively. Since these values indicate a quite similar interaction with the analyte, both QDs seem suitable for developing an analytical method for lamotrigine determination. To test which is the most suitable nanomaterial for detecting the lowest concentration of lamotrigine, we evaluated the influence of increasing lamotrigine concentration on the fluorescence of both WS_2-TD and WS_2-BU.

Figure 6A and B shows how the fluorescence of WS_2-TD and WS_2-BU, respectively, is quenched in the presence of

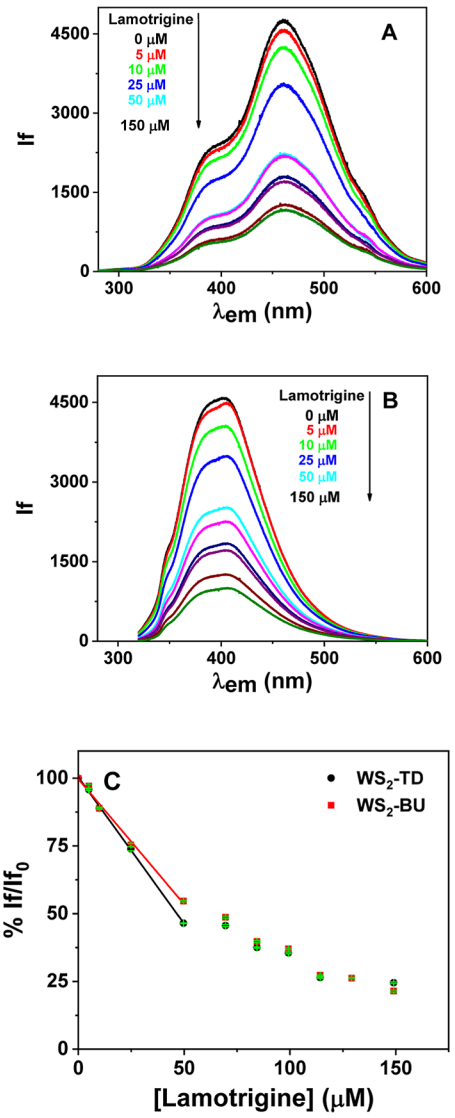

Figure 6. Fluorescence response of (A) WS_2-TD (λ_{ex} = 270 nm, λ_{em} = 460 nm) and (B) WS_2-BU (λ_{ex} = 310 nm, λ_{ex} = 400 nm) with increasing concentrations of lamotrigine. (C) Degree of inhibition (expressed as I_f/I_0, %) and lamotrigine concentration for WS_2-TD and WS_2-BU: calibration plots.

increasing concentrations of lamotrigine. In both cases, although a 150 μM lamotrigine concentration led to a fluorescence inhibition of about 80% of the initial signal, a linear correlation between the degree of inhibition (expressed as I_f/I_0, %) and lamotrigine concentration is obtained only up to a concentration of 50.0 μM (Figure 6C).

Table 1 summarizes the analytical parameters obtained for lamotrigine determination with both nanomaterials. As can be seen, the analytical method based on WS_2-TD is slightly more

https://doi.org/10.1021/acsomega.4c09476
ACS Omega 2025, 10, 17257−17268

Table 1. Analytical Parameters Obtained from the Calibration Plots for Lamotrigine Determination with WS_2-TD and WS_2-BU[ab]

WS_2 QDs	sensitivity (μM^{-1})	R	LOD (μM) (N = 3)	LOQ (μM) (N = 3)
WS2-TD	−1.08 ± 0.02	0.9996	5.68 ± 0.03	18.9 ± 0.2
WS2-BU	−0.92 ± 0.04	0.996	5.0 ± 0.1	17 ± 1

[a]The sensitivity is calculated from the slope of the calibration curve. Since increasing concentration for the lamotrigine results in the decrease in fluorescence intensity, a negative value is observed. [b]Sensitivity, correlation coefficient, detection limit (LOD), and quantification limit (LOQ).

sensitive, although it presents slightly higher detection and determination limits.

Study of the Mechanism of the Interaction of Lamotrigine and WS_2 QDs. A deep study of the quenching mechanism of WS_2 QDs by lamotrigine was carried out. As stated above, depending on the overlap of the absorption band of the quencher with the excitation or emission bands of the fluorophore, the mechanism will be different. When the absorption band overlaps with the emission fluorescence band, an energy transfer between the donor (fluorophore) and the acceptor (quencher) leads to fluorescence inhibition. In this case, the molecular structure of the analyte plays a role since it is important for the distance between the fluorophore and the analyte to be small. In our case, the planar structure of lamotrigine may facilitate this process. However, when the absorption band overlaps with the excitation band, a competition for the photons of the source occurs, causing fluorescence quenching. Since in our case the absorption band of the quencher overlaps with both the excitation and the emission bands of the nanomaterials, a mixed mechanism could be expected. In order to confirm this, the fluorescence inhibition was monitored by varying the lamotrigine concentration at two different excitation wavelengths. One is the wavelength where the WS_2-QDs present the maximum fluorescence and the lamotrigine absorbs (270 and 310 nm for WS_2-TD and WS_2-BU, respectively. See Figure 4). The other one is a wavelength at which the WS_2-QDs can be excited, but the analyte does not absorb (370 and 340 nm have been selected as λ_{ex} for WS_2-TD and WS_2-BU, respectively. See Figure 4). A fluorescence decrease in this condition would indicate the donor−acceptor energy mechanism. Figure S4 shows the results of this study. The quenching is produced at both wavelength conditions, leading to the conclusion that the mechanism is a mixture of both processes, with the photon competition being the predominant one as can be deduced by the higher inhibition produced when exciting at 270 and 310 nm for WS_2-TD and WS_2-BU, respectively. These results are similar to those obtained with other lamotrigine determination strategies that exhibit a competition inhibition mechanism.[45,46]

In addition to the steady-state quenching experiments, we also performed lifetime studies to establish the quenching mechanism between the QDs and the lamotrigine compound. Increasing the concentrations of lamotrigine did not show any changes in the fluorescence lifetime of the QDs. This indicates that the interaction is predominantly static, where the QDs form a complex with lamotrigine in the ground state. Figure S5 illustrates the fluorescence lifetime emission before and after the addition of 150 μM of lamotrigine. Table 2 presents the calculated lifetimes obtained from the best fit to a single-exponential decay model for the different QDs in each temporal profile.

Table 2. Lifetime Emission of the WS2-BU and WS_2-TD QDs before and after the Addition of Lamotrigine (150 μM)

sample	τ (ns)	R^2
WS_2-BU	5.97	0.99
WS_2-BU + 150 μM lamotrigine	5.91	0.99
WS_2-TD	2.24	0.98
WS_2-TD + 150 μM lamotrigine	2.23	0.98

Optical Sensor Development. Once the interaction of lamotrigine with WS_2 QDs was confirmed for both synthesized nanomaterials, we proceeded to immobilize the QDs on solid supports to develop an optical sensor for lamotrigine determination. To this end, two different supports have been selected, quartz plaques and circular filter papers.

The immobilization of WS_2 QDs on the quartz surface is carried out by the incorporation of the nanomaterial in a polymeric membrane. Although both WS_2-QDs are suitable for developing an analytical method in solution for lamotrigine determination, WS_2-TU was not suitable for this application due to the high background recorded when exciting the unmodified supports at 270 nm (data not shown). Moreover, as exciting at 310 nm is more selective for the analytical determination than at 270 nm, further studies were carried out with WS_2-BU.

Based on previous works, a polymeric membrane based on PVC with TBP as plasticizer was employed.[36,52] Since both the membrane and the support are optically transparent, they allow for instrumental analysis of compounds that undergo changes in the optical properties of the immobilized QDs. As described in the procedure section, the WS_2-BU were incorporated into the mixture composed of PVC and TBP in THF and then cast on the quartz plate by a spin coating procedure. Once the membrane is dried in an oven, the sensor is ready for use. Looking for the highest initial fluorescence signal in the dispositive, the volume of the WS_2-BU suspension employed for membrane preparation was optimized. Figure S6 shows the fluorescence spectra obtained with increasing volumes of dots in the PVC/THF/TBP mixture. As the WS_2-BU volume increases, the fluorescence emission band at 400 nm increases with respect to the blank membrane, reaching the maximum with 100 μL of nanomaterial. This response confirms the incorporation of the QDs in the polymeric membrane. Higher volumes of the aqueous WS_2-BU suspension led to PVC precipitation, making the polymeric mixture unsuitable to build the optical sensor.

To verify whether the inhibition of WS_2-BU fluorescence occurs once immobilized onto the quartz support, 20 μL of lamotrigine 1.00 mM was drop cast on top of the optical membrane and dried before recording the fluorescence spectrum. As shown in Figure 7A, the WS_2-BU fluorescence is quenched due to the addition of lamotrigine, confirming that the nanomaterial−analyte interaction also occurs on the membrane. Furthermore, this inhibition responds linearly with lamotrigine concentration until 250 μM according to the calibration equation: $\% I_f/I_{f0} = (100.0 \pm 0.3) - (0.258 \pm 0.005)$ [lamotrigine] (μM); r = 0.9994. The corresponding calibration plot is shown in Figure 7B. From these results, the detection limit (LOD) and the quantification limit (LOQ) were calculated as 3 and 10 σ/s, respectively, being σ the

https://doi.org/10.1021/acsomega.4c09476
ACS Omega 2025, 10, 17257−17268

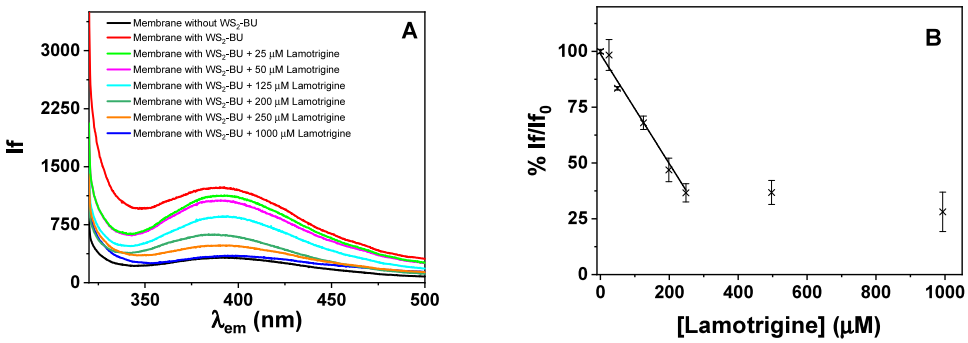

Figure 7. (A) On-surface WS_2-BU fluorescence quenching by lamotrigine. (B) Influence of lamotrigine concentration on the WS_2-BU fluorescence: calibration plot.

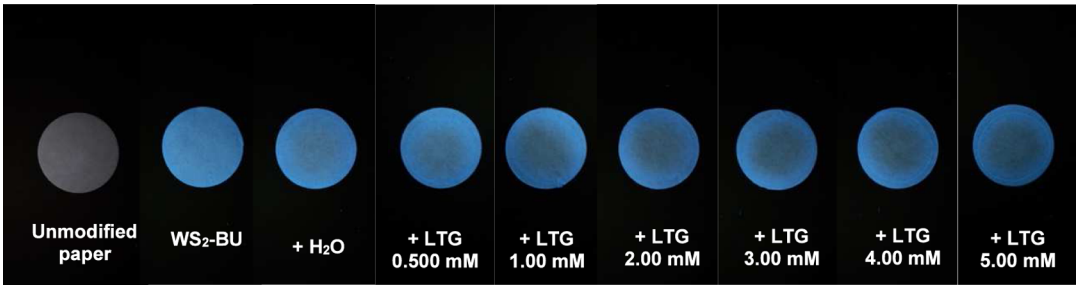

Figure 8. Images of analytical paper modified with WS_2-BU and increasing concentrations of lamotrigine (LTG).

standard deviation of the initial I_{f0} signals [n = 5] and s the slope of the calibration plot. Working in this way, a LOD value of 10.6 ± 0.6 μM and a LOQ of 35.4 ± 0.2 μM were obtained. In addition, the accuracy and the precision in terms of the relative error (Er, %) and for different sensors were evaluated for a lamotrigine concentration level of 200 μM. Five replicates were performed leading to a lamotrigine concentration of 205 ± 20 μM that corresponds to a relative standard deviation of 11% and Er values lower than 3% [n = 5]. These data allow us to conclude that the developed sensor shows very good results, in terms of accuracy and reproducibility. Table S1 compares the results obtained in this work with those reported in the literature. Although some methods show better performance than those presented in this work, it is important to note that the analytical determination of lamotrigine in these methods is carried out in solution, whereas this work focuses on surface-based detection.

The sensor was applied to the lamotrigine determination in synthetic human serum by a standard addition method. Due to the absence of the analyte in the sample, human serum was spiked with lamotrigine at a concentration of 50 μM before being filtered through a 0.45 μm filter. The % I_f/I_{f0} signal changed with the added lamotrigine concentration according to the equation % I_f/I_{f0} = (83.2 ± 0.9) − (0.36 ± 0.03) $[\text{lamotrigine}]_{\text{added}}$ (μM); r = 0.997. From these results, a lamotrigine concentration of 47 μM was obtained, which means a recovery of 94%.

Finally, we have employed circular filter paper as support for immobilizing TMD dots to test the suitability of this support to develop rapid and visual detection methods for noncolored analytes. To this end, the paper was modified with WS_2-BU and subsequently 25.0 μL of the analyte was dropped onto the central region of the support. Following irradiation under a 365 nm lamp, images of all of the different paper samples were recorded, as depicted in Figure 8. The images reveal that an increasing concentration of the analyte produces the inhibition of the WS_2-BU dots fluorescence. These results confirm the possibility of employing this nanomaterial for the development of interesting sensors on paper.

CONCLUSIONS

We synthesized WS_2 QDs by two different approaches: top-down (WS_2-TD) and bottom-up (WS_2-BU). From the AFM measurements of the samples deposited on mica, the QDs height distribution is obtained, which follows quite well the lognormal distribution for the WS_2-BU system whereas that of the WS_2-TD shows larger counts for dot heights above the average value, which could be related with their different optical behavior. It should be noted that the height values measured by AFM underestimate the real values since the QDs are embedded within a background layer formed on the mica surface. Both WS_2-QDs present native fluorescence, with maximum of emissions at 460 and 400 nm when they are excited at 270 and 310 nm, for WS_2-TD and WS_2-BU, respectively. This fluorescence is inhibited in the presence of the antiepileptic drug lamotrigine through a mixed mechanism: a donor−acceptor energy mechanism and the competition for the photons coming from the excitation source, the latter being the predominant one. Both nanomaterials exhibit similar interaction with lamotrigine, with K_{SV} values of 20,431 and 17,556 M^{-1} for WS_2-TD and WS_2-BU, respectively. The fluorescence of the QDs is inhibited by increasing concentrations of lamotrigine, showing a linear correlation up to 50.0 μM in both cases. Moreover, this behavior is maintained when both WS_2-QDs are immobilized onto quartz plates, allowing the development of an optical sensor, with a detection limit of 10.6 μM, which was successfully applied to the determination of lamotrigine in synthetic human serum. Finally, it was proven that paper is also a suitable support for developing rapid and visual detection methods for noncolored analytes.

https://doi.org/10.1021/acsomega.4c09476
ACS Omega 2025, 10, 17257−17268

■ ASSOCIATED CONTENT

Supporting Information

The Supporting Information is available free of charge at https://pubs.acs.org/doi/10.1021/acsomega.4c09476.

Additional information related to morphological and optical characterization of WS_2-QDs as well as measurements for the study of inhibition mechanisms; and comparison with other methods (PDF)

■ AUTHOR INFORMATION

Corresponding Author

María del Pozo − *Departamento de Química Analítica y Análisis Instrumental. Facultad de Ciencias. c/Francisco Tomás y Valiente, No 7. Campus de Excelencia de la Universidad Autónoma de Madrid, Madrid 28049, Spain;* orcid.org/0000-0003-2791-8316; Email: maria.delpozo@uam.es

Authors

Lina Hristova − *Departamento de Química Analítica y Análisis Instrumental. Facultad de Ciencias. c/Francisco Tomás y Valiente, No 7. Campus de Excelencia de la Universidad Autónoma de Madrid, Madrid 28049, Spain*

Rut Martínez-Moro − *Departamento de Química Analítica y Análisis Instrumental. Facultad de Ciencias. c/Francisco Tomás y Valiente, No 7. Campus de Excelencia de la Universidad Autónoma de Madrid, Madrid 28049, Spain*

Esperanza Fernández-García − *Departamento de Química Analítica y Análisis Instrumental. Facultad de Ciencias. c/Francisco Tomás y Valiente, No 7. Campus de Excelencia de la Universidad Autónoma de Madrid, Madrid 28049, Spain;* orcid.org/0000-0001-9785-3349

Luis Vázquez − *CSIC. c/Sor Juana Inés de la Cruz No 3. Campus de Excelencia de la Universidad Autónoma de Madrid, Instituto de Ciencia de Materiales de Madrid (ICMM), Madrid 28049, Spain;* orcid.org/0000-0001-6220-2810

Pedro Atienzar − *CSIC-UPV, Universitat Politècnica de València, Avenida de los Naranjos S/N. Campus Universitat Politècnica de València, Instituto de Tecnología Química, Valencia 46022, Spain;* orcid.org/0000-0002-0356-021X

María Dolores Petit-Domínguez − *Departamento de Química Analítica y Análisis Instrumental. Facultad de Ciencias. c/Francisco Tomás y Valiente, No 7. Campus de Excelencia de la Universidad Autónoma de Madrid, Madrid 28049, Spain*

Elena Casero − *Departamento de Química Analítica y Análisis Instrumental. Facultad de Ciencias. c/Francisco Tomás y Valiente, No 7. Campus de Excelencia de la Universidad Autónoma de Madrid, Madrid 28049, Spain*

Carmen Quintana − *Departamento de Química Analítica y Análisis Instrumental. Facultad de Ciencias. c/Francisco Tomás y Valiente, No 7. Campus de Excelencia de la Universidad Autónoma de Madrid, Madrid 28049, Spain;* orcid.org/0000-0002-3879-848X

Complete contact information is available at: https://pubs.acs.org/10.1021/acsomega.4c09476

Notes

The authors declare no competing financial interest.

■ ACKNOWLEDGMENTS

The authors acknowledge financial support from projects PID2020-113142RB-C21, PID2020-113142RB-C22, PID2023-149077OB-C32, and PID2023-149077OB-C31 funded by MCIN/AEI/10.13039/501100011033. This research was also funded by the ITQ though the project PID2021-123163OB-I00 funded by MCIN/AEI/10.13039/501100011033/and FEDER A way of making Europe and Severo Ochoa Centre of excellence program (CEX2021-001230-S). We thank to Jaime Martín Benito for his help in the characterization measurements discussion.

■ REFERENCES

(1) Gupta, A.; Sakthivel, T.; Seal, S. Recent Development in 2D Materials beyond Graphene. *Prog. Mater. Sci.* **2015**, *73*, 44−126.

(2) Justino, C. I. L.; Gomes, A. R.; Freitas, A. C.; Duarte, A. C.; Rocha-Santos, T. A. P. Graphene Based Sensors and Biosensors. *Trends Anal. Chem.* **2017**, *91*, 53−66.

(3) Choi, W.; Choudhary, N.; Han, G. H.; Park, J.; Akinwande, D.; Lee, Y. H. Recent Development of Two-Dimensional Transition Metal Dichalcogenides and Their Applications. *Mater. Today* **2017**, *20*, 116−130.

(4) Rahman, M. T.; Kumar, R.; Kumar, M.; Qiao, Q. Two-Dimensional Transition Metal Dichalcogenides and Their Composites for Lab-Based Sensing Applications: Recent Progress and Future Outlook. *Sens. Actuators, A* **2021**, *318*, 112517.

(5) Zhao, B.; Shen, D.; Zhang, Z.; Lu, P.; Hossain, M.; Li, J.; Li, B.; Duan, X. 2D Metallic Transition-Metal Dichalcogenides: Structures, Synthesis, Properties, and Applications. *Adv. Funct. Mater.* **2021**, *31*, 2105132.

(6) Tajik, S.; Dourandish, Z.; Garkani Nejad, F.; Beitollahi, H.; Jahani, P. M.; Di Bartolomeo, A. Transition Metal Dichalcogenides: Synthesis and Use in the Development of Electrochemical Sensors and Biosensors. *Biosens. Bioelectron.* **2022**, *216*, 114674.

(7) Cao, X.; Ding, C.; Zhang, C.; Gu, W.; Yan, Y.; Shi, X.; Xian, Y. Transition Metal Dichalcogenide Quantum Dots: Synthesis, Photoluminescence and Biological Applications. *J. Mater. Chem. B* **2018**, *6*, 8011−8036.

(8) Singh, V. K.; Mishra, H.; Ali, R.; Umrao, S.; Srivastava, R.; Abraham, S.; Misra, A.; Singh, V. N.; Mishra, H.; Tiwari, R. S.; et al. In Situ Functionalized Fluorescent WS_2-QDs as Sensitive and Selective Probe for Fe^{3+} and a Detailed Study of Its Fluorescence Quenching. *ACS Appl. Nano Mater.* **2019**, *2*, 566−576.

(9) Gu, W.; Yan, Y.; Cao, X.; Zhang, C.; Ding, C.; Xian, Y. A Facile and One-Step Ethanol-Thermal Synthesis of MoS_2 Quantum Dots for Two-Photon Fluorescence Imaging. *J. Mater. Chem. B* **2016**, *4*, 27−31.

(10) Splendiani, A.; Sun, L.; Zhang, Y.; Li, T.; Kim, J.; Chim, C. Y.; Galli, G.; Wang, F. Emerging Photoluminescence in Monolayer MoS_2. *Nano Lett.* **2010**, *10*, 1271−1275.

(11) Eda, G.; Yamaguchi, H.; Voiry, D.; Fujita, T.; Chen, M.; Chhowalla, M. Photoluminescence from Chemically Exfoliated MoS_2. *Nano Lett.* **2011**, *11*, 5111−5116.

(12) Hang, D. R.; Sun, D. Y.; Chen, C. H.; Wu, H. F.; Chou, M. M. C.; Islam, S. E.; Sharma, K. H. Facile Bottom-up Preparation of WS_2-Based Water-Soluble Quantum Dots as Luminescent Probes for Hydrogen Peroxide and Glucose. *Nanoscale Res. Lett.* **2019**, *14*, 271.

(13) Salavagione, H. J.; Sherwood, J.; De Bruyn, M.; Budarin, V. L.; Ellis, G. J.; Clark, J. H.; Shuttleworth, P. S. Identification of High Performance Solvents for the Sustainable Processing of Graphene. *Green Chem.* **2017**, *19*, 2550−2560.

(14) Hyun, D.; Kim, J.; Ko, H.; Shin, Y.; Park, J.; Bak, S.; Lee, J.; Yang, J.; Boo, J. H.; Lee, H. One-Step Synthesis of Transition Metal Dichalcogenide Quantum Dots Using Only Alcohol Solvents for Indoor-Light Photocatalytic Antibacterial Activity. *ACS Appl. Bio Mater.* **2023**, *6*, 1970−1980.

(15) Guo, Y.; Li, J. MoS_2 Quantum Dots: Synthesis, Properties and Biological Applications. *Mater. Sci. Eng., C* **2020**, *109*, 110511−110513.
(16) Gu, W.; Yan, Y.; Zhang, C.; Ding, C.; Xian, Y. One-Step Synthesis of Water-Soluble MoS_2 Quantum Dots via a Hydrothermal Method as a Fluorescent Probe for Hyaluronidase Detection. *ACS Appl. Mater. Interfaces* **2016**, *8*, 11272−11279.
(17) Chen, S.; Yu, Y. L.; Wang, J. H. Inner Filter Effect-Based Fluorescent Sensing Systems: A Review. *Anal. Chim. Acta* **2018**, *999*, 13−26.
(18) Coloma, A.; del Pozo, M.; Martínez-Moro, R.; Blanco, E.; Atienzar, P.; Sánchez, L.; Petit-Domínguez, M. D.; Casero, E.; Quintana, C. MoS_2 Quantum Dots for On-Line Fluorescence Determination of the Food Additive Allura Red. *Food Chem.* **2021**, *345*, 128628.
(19) Yang, L.; Ge, J.; Ma, D.; Tang, J.; Wang, H.; Li, Z. MoS_2 Quantum Dots as Fluorescent Probe for Methotrexate Detection. *Spectrochim. Acta, Part A* **2022**, *279*, 121443.
(20) Sathyan, B.; Tomy, A. M.; Pm, N.; Cyriac, J. A Facile Strategy of Using MoS_2 Quantum Dots for Fluorescence-Based Targeted Detection of Nitrobenzene. *RSC Adv.* **2023**, *13*, 14614−14624.
(21) Wu, F. Y.; Yang, J. L.; Ye, Y. S.; Kong, Y. Q.; Wu, R.; Wang, H. Y.; Wang, X. Polychromatic Fluorescent MoS_2 Quantum Dots: Fabrication and off-on Sensing for Fluorine Ions in Water. *Anal. Methods* **2023**, *15*, 2490−2496.
(22) Duan, X.; Li, N.; Wang, G.; Su, X. High Sensitive Ratiometric Fluorescence Analysis of Trypsin and Dithiothreitol Based on WS_2 QDs. *Talanta* **2020**, *219*, 121171.
(23) Haghighi, L.; Haghnazari, N.; Karami, C. Tungsten Disulfide Quantum Dots (WS_2 QDs) as a Fluorescence Probe for Detection of Dopamine (DA). *J. Mater. Sci.: Mater. Electron.* **2021**, *32*, 28042−28050.
(24) Aneesha; Ohta, N.; Mehata, M. S. In Situ Synthesis of WS_2 QDs for Sensing of H_2O_2: Quenching and Recovery of Absorption and Photoluminescence. *Mater. Today Commun.* **2023**, *34*, 105013.
(25) Guo, X.; Wang, Y.; Wu, F.; Ni, Y.; Kokot, S. The Use of Tungsten Disulfide Dots as Highly Selective, Fluorescent Probes for Analysis of Nitrofurazone. *Talanta* **2015**, *144*, 1036−1043.
(26) Bora, S.; Upadhyay, C. Highly Efficient WS_2 QD-Based Non-Enzymatic Fluorescent Biosensor for Ofloxacin and Ciprofloxacin Monitoring in Aquatic Media. *Sens. Diagn.* **2024**, *3*, 1522−1532.
(27) Azizi, N.; Hallaj, T.; Samadi, N. A Dual-Mode Fluorometric and Smartphone-Based Colorimetric Sensor for Cyanide Detection Using Tungsten Disulfide Quantum Dots and Silver Nanoparticles. *J. Food Compos. Anal.* **2024**, *129*, 106081.
(28) Sun, Y.; Liu, W.; Chen, M.; Ji, H.; Jiang, M.; Hao, Z.; Li, X.; He, S.; Zhang, L.; Zhang, R. Non-Enzymatic Signal-on Electrochemiluminescence Detection of Organophosphorus Pesticides Based on Tungsten Disulfide Quantum Dots. *Green Chem.* **2024**, *26*, 7123−7131.
(29) Haddad Irani-nezhad, M.; Jalili, R.; Kohan, E.; Khataee, A.; Yoon, Y. Tungsten Disulfide (WS_2)/Fluorescein Ratiometric Fluorescent Probe for Detection of Cefixime Residues in Milk. *Environ. Res.* **2022**, *205*, 112512.
(30) Ghasemi, F.; Fahimi-Kashani, N.; Bigdeli, A.; Alshatteri, A. H.; Abbasi-Moayed, S.; Al-Jaf, S. H.; Merry, M. Y.; Omer, K. M.; Hormozi-Nezhad, M. R. Paper-Based Optical Nanosensors—A Review. *Anal. Chim. Acta* **2023**, *1238*, 340640.
(31) Di Nonno, S.; Ulber, R. Smartphone-Based Optical Analysis Systems. *Analyst* **2021**, *146*, 2749−2768.
(32) Jiang, L.; Ye, H.; Ma, D.; Rodrigues, J.; Sheng, R.; Min, D. A Smartphone-Adaptable Fluorescent Sensing Tag for Non-Contact and Visual Monitoring of the Freshness of Fish. *Analyst* **2022**, *147*, 923−931.
(33) Zhu, H.; Zhang, H.; Xia, Y. Planar Is Better: Monodisperse Three-Layered MoS_2 Quantum Dots as Fluorescent Reporters for 2,4,6-Trinitrotoluene Sensing in Environmental Water and Luggage Cases. *Anal. Chem.* **2018**, *90*, 3942−3949.
(34) Guo, X.; Huang, J.; Wei, Y.; Zeng, Q.; Wang, L. Fast and Selective Detection of Mercury Ions in Environmental Water by Paper-Based Fluorescent Sensor Using Boronic Acid Functionalized MoS_2 Quantum Dots. *J. Hazard. Mater.* **2020**, *381*, 120969.
(35) Wang, X.; Hou, J.; Lan, S.; Shen, C.; Huo, D.; Ji, Z.; Ma, Y.; Luo, H.; Zhang, S.; He, Q.; et al. MoS_2 QDs-Based Sensor for Measurement of Fluazinam with Triple Signal Output. *Anal. Chim. Acta* **2020**, *1108*, 152−159.
(36) Martínez-Moro, R.; del Pozo, M.; Casero, E.; Petit-Domínguez, M. D.; Quintana, C. MoS_2 Quantum Dots-Based Optical Sensing Platform for the Analysis of Synthetic Colorants. Application to Quinoline Yellow Determination. *Spectrochim. Acta, Part A* **2023**, *302*, 123042.
(37) Guo, M.; Shao, L.; Du, Y.; Qian, Z.; Huang, T.; Tang, D. Microporous Polymer Based on the New Compound "Bi-(4-Vinyl Phenylquinoline) Amide" for Enrichment and Quantitative Determination of Lamotrigine in Rat and Human Serum. *Anal. Bioanal. Chem.* **2019**, *411*, 3353−3360.
(38) Jin, S.; Zhao, Q.; Zhang, D.; Zhao, Z.; Mei, S. Development and Validation of an Improved HPLC-UV Method for Simultaneous Determination of Lamotrigine and Oxcarbazepine and Its Active Metabolite 10,11-Dihydro-10-Hydroxycarbazepine in Human Blood Plasma and Comparison with an UHPLC-MS/MS Method. *J. Anal. Sci. Technol.* **2019**, *10*, 36.
(39) Parvin, S.; Aghamohammadi, M.; Fallahi, E.; Kalhor, H. Simultaneous Determination of Lamotrigine and Carbamazepine in Plasma Using Ultrasound-Assisted Emulsification Microextraction-High Performance Liquid Chromatography. *J. Anal. Chem.* **2020**, *75*, 622−628.
(40) Zhang, Y. Y.; Xia, Y.; Guo, H. L.; Hu, Y. H.; Wen, X. Y.; Chen, J.; Lu, X. P.; Wang, S. S.; Qiu, J. C.; Chen, F. An LC−ESI−MS/MS Assay for the Therapeutic Drug Monitoring of 15 Antiseizure Medications in Plasma of Children with Epilepsy. *Biomed. Chromatogr.* **2022**, *36*, No. e5484.
(41) Gondhale-Karpe, P.; Manwatkar, S. Quantitative Determination of Related Substances for Lamotrigine Extended Release Tablet by RP-HPLC. *Heliyon* **2023**, *9*, No. e15732.
(42) Wang, H.; Qian, D.; Xiao, X.; Gao, S.; Cheng, J.; He, B.; Liao, L.; Deng, J. A Highly Sensitive and Selective Sensor Based on a Graphene-Coated Carbon Paste Electrode Modified with a Computationally Designed Boron-Embedded Duplex Molecularly Imprinted Hybrid Membrane for the Sensing of Lamotrigine. *Biosens. Bioelectron.* **2017**, *94*, 663−670.
(43) Ciucu, A. A.; Buleandră, M.; Ciurea, T.; Stoica, V. N.; Ştefanescu, C. D.; Ciobanu, A. A New Voltammetric Approach for Electrochemical Determination of Lamotrigine in Pharmaceutical Samples. *Electroanalysis* **2021**, *33*, 1389−1392.
(44) El-Enany, N. M.; El-Sherbiny, D. T.; Abdelal, A. A.; Belal, F. F. Validated Spectrofluorimetric Method for the Determination of Lamotrigine in Tablets and Human Plasma through Derivatization with O-Phthalaldehyde. *J. Fluoresc.* **2010**, *20*, 463−472.
(45) Song, D.; Ji, X.; Li, Y.; Chen, S.; Wu, S.; Zhang, Y.; Gao, E.; Zhu, M. A Terbium-Based Coordination Polymer for Sensitive Ratiometric Fluorescence Detection of Lamotrigine. *J. Lumin.* **2022**, *251*, 119129.
(46) Sun, X. C.; Zhu, M. C.; Wu, S. Y.; Zhang, Y.; Bai, X. J. Nitrogen-Containing Lanthanide Metal-Organic Framework Nanostructure for Fluorescent Detection of Lamotrigine. *ACS Appl. Nano Mater.* **2022**, *5*, 8723−8729.
(47) Eydi, P.; Rahimpour, E.; Khoubnasabjafari, M.; Jouyban-Gharamaleki, V.; Jouyban, A. A Terbium Metal-Organic Framework Platform for Determination of Lamotrigine in Exhaled Breath Condensate. *Pharm. Sci.* **2021**, *28*, 572−578.
(48) Bazrafshan, E.; Dadfarnia, S.; Haji Shabani, A. M.; Afsharipour, R. Determination of Lamotrigine by Fluorescence Quenching of N-Doped Graphene Quantum Dots after Its Solid-Phase Extraction Using Magnetic Graphene Oxide. *Spectrochim. Acta, Part A* **2022**, *267*, 120530.

https://doi.org/10.1021/acsomega.4c09476
ACS Omega 2025, 10, 17257−17268

(49) Jouyban, A.; Samadi, A.; Khoubnasabjafari, M. A New "Turn-on" Fluorescent Sensor Based on Gold Quantum Dots and Silver Nanoparticles for Lamotrigine Detection in Plasma. *Talanta* **2017**, *172*, 126−132.
(50) Xu, S.; Li, D.; Wu, P. One-Pot, Facile, and Versatile Synthesis of Monolayer MoS_2 /WS_2 Quantum Dots as Bioimaging Probes and Efficient Electrocatalysts for Hydrogen Evolution Reaction. *Adv. Funct. Mater.* **2015**, *25*, 1127−1136.
(51) Nečas, D.; Klapetek, P. Gwyddion An Open-Source Software for SPM Data Analysis. *Cent. Eur. J. Phys.* **2012**, *10*, 181−188.
(52) Jiménez, J.; Blasco, S.; Blanco, E.; Atienzar, P.; del Pozo, M.; Quintana, C. On-Surface Cucurbit[n]Uril Supramolecular Recognition for an Optical Sensor Design. *ChemistrySelect* **2019**, *4*, 7036−7041.
(53) Tang, S.; You, X.; Fang, Q.; Li, X.; Li, G.; Chen, J.; Chen, W.; Chen, W. A Fluorescence Inner-Filter Effect Based Sensing Platform for Turn-On Detection of Glutathione in Human Serum. *Sensors* **2019**, *19*, 228.
(54) Hu, L.; Zhang, Q.; Gan, X.; Yin, W.; Fu, W. Switchable Fluorescence of MoS_2 Quantum Dots: A Multifunctional Probe for Sensing of Chromium(VI), Ascorbic Acid, and Alkaline Phosphatase Activity. *Anal. Bioanal. Chem.* **2018**, *410*, 7551−7557.
(55) Kiss, L. B.; Söderlund, J.; Niklasson, G. A.; Granqvist, C. G. New Approach to the Origin of Lognormal Size Distributions of Nanoparticles. *Nanotechnology* **1999**, *10*, 25−28.
(56) Laube, J.; Gutsch, S.; Wang, D.; Kübel, C.; Zacharias, M.; Hiller, D. Two-Dimensional Percolation Threshold in Confined Si Nanoparticle Networks. *Appl. Phys. Lett.* **2016**, *108*, 043106.

https://doi.org/10.1021/acsomega.4c09476
ACS Omega 2025, 10, 17257−17268